Effect of the Dipole–Dipole Interactions in the Molecular Dynamics of Poly(vinylpyrrolidone)-Based Copolymers

ARTICLE *in* MACROMOLECULES · JULY 2014

Impact Factor: 5.8

7 AUTHORS, INCLUDING:

Pilar Ortiz-Serna

Universitat Politècnica de València

17 PUBLICATIONS **51** CITATIONS

SEE PROFILE

M.J. Sanchis

Universitat Politècnica de València

106 PUBLICATIONS **870** CITATIONS

SEE PROFILE

Saúl Vallejos

Universidad de Burgos

17 PUBLICATIONS **118** CITATIONS

SEE PROFILE

Jose Miguel Garcia

Universidad de Burgos

85 PUBLICATIONS **1,263** CITATIONS

SEE PROFILE

Macromolecules

Article

pubs.acs.org/Macromolecules

Effect of the Dipole–Dipole Interactions in the Molecular Dynamics of Poly(vinylpyrrolidone)-Based Copolymers

B. Redondo-Foj,[†] M. Carsí,[†] P. Ortiz-Serna,[†] and M. J. Sanchis[†,*]

[†]Instituto Tecnológico de la Energía, Departamento de Termodinámica Aplicada, Universitat Politècnica de València, Camí de Vera s/n, 46022, Valencia, Spain

S. Vallejos,[‡] F. García,[‡] and J. M. García[‡]

[‡]Departamento de Química, Facultad de Ciencias, Universidad de Burgos, Plaza Misael Bañuelos s/n, 09001 Burgos, Spain

ABSTRACT: Poly(vinylpyrrolidone-*co*-butyl acrylate) samples with different proportions of monomers were prepared as tractable and hydrophilic materials. An analysis of the intermolecular interactions between the polymer groups was carried out by FTIR. The dependence of the C═O bands (lactam and pendant butyl ester) with the composition suggests a strong interaction between the lactam groups. They exert an important influence in the molecular mobility, which was studied by DSC and DRS. A single narrow glass transition temperature (T_g) is observed in each random copolymer, consistent with a single phase of low compositional nanoheterogeneity. The dependence of the T_g with the composition suggests significant interactions between polymer components. The dielectric spectra show γ, β, and α relaxations in increasing order of temperature, followed by conductive contributions. The apparent activation energies for secondary relaxations have similar values for all the samples. The γ-process is related to the local motions of the butyl units and the β-process is a Johari–Golstein secondary relaxation that is related to the local motions of the pyrrolidone group together with the motion of polymer backbone segments.

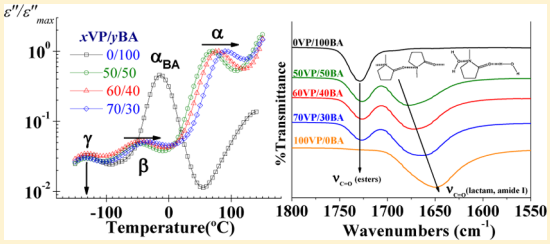

1. INTRODUCTION

N-Vinyl-2-pyrrolidone (VP) is a cheap and widely available chemical, prepared industrially from acetylene and formaldehyde following the Reppe's procedure.[1,2] VP is a high boiling point liquid (92–95 °C at 1.3 kPa), highly miscible in water and in organic solvents, and with other vinyl or acrylic monomers. VP linear polymerization, either in bulk, in solution or in suspension, gives rise to linear polyvinylpirrolidone (PVP). PVP is also known as Povidone, an amphiphilic polymer soluble in water and in polar organic solvents but insoluble in esters, ethers, ketones and hydrocarbons.[3] It cannot be melt processed due to its low decomposition temperature. Its T_g reaches a constant value (approximately 175 °C) when its average molecular weight is 100 000 g·mol^{-1}.[4] The films prepared from PVP solution are brittle, clear, and glossy. Its popcorn polymerization, i.e., proliferous polymerization, gives rise to highly cross-linked PVP, called Crospovidone, completely insoluble, and of the great industrial importance. Both, linear and cross-linked PVP have a wide range of applications. Because of its biocompatibility, PVP is used in pharmacological and biomedical applications. Furthermore, it is also utilized in numerous industrial fields like adhesives, ceramic, coatings, food, etc.[2,3]

The relation between the structure of polymers and their properties has been widely studied in the literature. In this way, the copolymerization is presented as an effective method to prepare macromolecules with specific chemical structures and to control some properties such as hydrophilic/hydrophobic balances, solubility, polarity, etc.[5] Hence, copolymers have attracted a great attention because they can be frequently used to tune the properties of a material between those of the corresponding homopolymers. Copolymers comprised of VP and acrylic or vinyl comonomers are commercially produced to modify, to improve and to adapt the properties of PVP to specific applications. In the same way, the water affinity of the PVP, or even the water solubility, which can be too high for certain applications, has been reduced by copolymerizing with vinyl acetate or vinyl propionate.[3,6] Thus, acrylic chemicals are among the most versatile and inexpensive comonomers to prepare materials with specific properties.

The dynamic mechanical and dielectrical properties are intrinsically correlated and they are associated with a structural polymer feature.[7−12] The dynamic relaxation properties of cross-linked polymer networks are highly sensitive to network composition and polymer chain architecture. The cooperative segmental motions (T_g) and the more localized processes observed below T_g, can be dramatically affected by (i) changes in the backbone structure, (ii) cross-link density, or (iii) the introduction of pendant groups or branches. One of the most powerful and versatile methods for the study of molecular

Received: April 16, 2014
Revised: July 8, 2014
Published: July 18, 2014

   dx.doi.org/10.1021/ma500800a | *Macromolecules* 2014, 47, 5334–5346

dynamics in polymer networks is the dielectric relaxation spectroscopy (DRS).[13] DRS is now widely used to investigate molecular dynamics of copolymers and nanocomposites.[14]

Thus, we have prepared and characterized PVP-based copolymers using the highly hydrophobic butyl acrylate (BA) as comonomer in different molar proportion. Some reasons for the use BA as the comonomer are (i) the VP/acrylic copolymers have a known chemical microstructure, in terms of triad and tetrad composition sequences;[15,16] (ii) BA is fully miscible with VP; (iii) BA is a highly hydrophobic monomer which counterbalances the highly hydrophilic character of VP and (iv) the BA homopolymer is an extremely soft material,[17] with T_g = −54 °C, which permits to modulate the characteristic brittleness of VP homopolymer, thus obtaining more tractable materials.

A study of the *x*VP/*y*BA copolymer family behavior regarding several parameters would permit to establish the structure-properties relationships and to optimize the performance according to a needed application. In a previous work of our research group, the thermal, mechanical and dielectric properties of poly(vinylpyrrolidone-*co*-butyl acrylate) with a molar ratio of 60:40 was studied.[9] That study was mainly focused on the analysis and comparison of the copolymer response to dynamic electrical and mechanical fields. The present paper includes the analysis of the chemical and physical properties of a series of novel *x*VP/*y*BA copolymer samples using several experimental techniques. In this study, a deep comparative analysis between different characterization techniques and copolymer compositions is carried out.

2. EXPERIMENTAL PART

Sample Preparation. All chemicals were commercially obtained and used as received: 1-Vinyl-2-pyrrolidone (VP) (Aldrich, 99%), butyl acrylate (BA) (Fluka, 99.5%), ethylene glycol dimethacrylate (EGDMMA) (Aldrich, 98%), and 2,2-dimethoxy-2-phenylacetophenone (Aldrich, 99%). Samples of poly(vinylpyrrolidone-*co*-butyl acrylate) were prepared by radical polymerization of VP and butyl acrylate BA mixture with a molar ratio of 100:0, 70:30, 60:40, 50:50, and 0:100. EGDMMA was used as the cross-linking agent. The molar ratio of cross-linker to the other comonomers, VP and BA, was 1%. 2-Dimethoxy-2-phenylacetophenone (1.6 wt %) was used as a radical photoinitiator. The homogeneous solution comprised of VP, BA, and EGDMMA, and the photoinitiator were transferred to an ampule, degassed by nitrogen bubbling for 15 min, and injected into an oxygen-free atmosphere. The photoinitiated bulk polymerization was performed in a 100 μm thick silanized glass hermetic mold upon irradiation with a UV mercury lamp (250w, Philips HPL-N, emission band in the UV region at 304, 314, 335, and 366 nm, with maximum emission at 366 nm), at 20 °C, for 1 h. The sample containing only BA and EGDMMA was prepared using a 300 μm thick silanized glass hermetic mold, in order to obtain a tractable material, due to its softness. Then, the samples were conditioned by means of a thoroughly wash with acetone (two washing cycles each of 3 h) followed by a drying process at room temperature and a dip into pure water overnight. Finally, they were dried in a vacuum oven at 20 °C. The chemical constitution of the polymer samples, along with the molar ratio of comonomers VP, BA, and EGDMMA, is depicted in Table 1.

Sample Hydrophilicity Characterization. The *x*VP/*y*BA samples were immersed in pure water at 20 °C until reaching the swelling equilibrium (constant weight). After that, they were weighted (w_s), dried in an air-circulating oven at 60 °C for 2 h, and weighted again (w_d). Then, the water-swelling percentage (WSP) was calculated, where WSP is defined as the weight percentage of water uptake when the film is soaked until equilibrium in pure water. It is obtained as follows: $100(w_s - w_d)/w_d$.

Table 1. Chemical Structures of the Comonomers and of the Dense Copolymer Samples

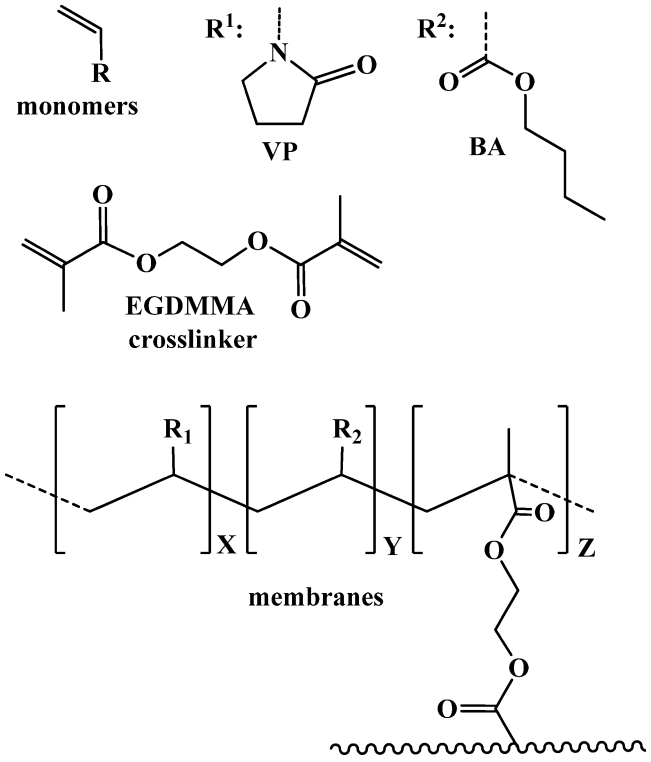

sample code	monomer molar ratio		
	x	*y*	*z*
100VP/0BA	100	0	1
70VP/30BA	70	30	1
60VP/40BA	60	40	1
50VP/50BA	50	50	1
0VP/100BA	0	100	1

Fourier Transform Infrared Measurements (FTIR). Infrared spectra (FTIR) of dried *x*VP/*y*BA samples were recorded with a JASCO FT/IT-4100 fitted with a PIKE TECH "Miracle" ATR accessory.

Thermogravimetric Analysis (TGA). Thermogravimetric analysis (TGA) data of *x*VP/*y*BA samples were obtained for dried samples of 5 mg under nitrogen flow, using a TA Instruments Q50 TGA analyzer at a scan rate of 10 °C·min^{-1}.

Modulated Differential Scanning Calorimetry Measurements (MDSC). Modulated differential scanning calorimetry (MDSC) of *x*VP/*y*BA samples was carried out using a TA Instruments DSC Q-20 with a refrigerated cooling system. The DSC tests were performed under a 50 mL·min^{-1} flow of nitrogen to prevent oxidation. High-purity indium was used to calibrate the cell. The thin films were repeatedly stacked into a pan, with a weight of approximately 7.0 mg. The measurements were conducted in crimpled nonhermetic aluminum pans, using an empty crimpled aluminum pan as the reference cell. Standard modulation conditions used in the experiments were 1 °C of amplitude and 60 s of period. Each measurement was taken in two cycles from −80 to +200 °C at a heating rate of 3 °C·min^{-1}. The first run was carried out in order to remove all the residual moisture and the thermal history. The T_g was evaluated as the intersection of the baseline of the glassy region with the tangent to the endotherm in the middle point.

Mechanical Properties. The tensile properties of the *x*VP/*y*BA samples were analyzed using a Hounsfield H10KM Universal Testing Dynamometer. Strips were cut from the polymer films with 5 mm of width, 30 mm of length, and 100−120 μm of thick. The samples were dried at 90 °C for 1 h and then measured at 30 °C with an extension

dx.doi.org/10.1021/ma500800a | Macromolecules 2014, 47, 5334−5346

Table 2. Film Sample Characteristics [Thickness, Water Swelling Percentage (WSP), Thermal Resistance, and Mechanical Properties]

			TGA (N_2 atmosphere)		Mechanical properties		
sample	sample thickness (μm)	WSP (%)	T_5 (°C)	T_{10} (°C)	Young modulus (MPa)	tensile strength (MPa)	elongation (%)
100VP/0BA	115	>200	378	395	1476[a]	31[a]	7[a]
70VP/30BA	123	92	350	367	455[a]	20[a]	458[a]
60VP/40BA	115	60	349	370	200[a]	15[a]	540[a]
50VP/50BA	111	37	353	367	60[b]	15[b]	780[b]
0VP/100BA	290	<1	295	332	*c*	*c*	*c*

[a]Extension rate of 5 mm·min^{-1}. [b]Extension rate of 10 mm·min^{-1}. [c]The mechanical analysis could not be carried out because of the softness of the material, even with a thickness of 290 μm.

rate of 5 or 10 mm·min^{-1} and a gauge length of 10 mm. At least six samples were tested for each polymer in order to average the obtained data.

Broadband Dielectric Relaxation Spectroscopy (DRS). Isothermal relaxation spectra of *x*VP/*y*BA samples were collected by using a Novocontrol Broadband Dielectric Spectrometer (Hundsagen, Germany) consisting of an Alpha analyzer to carry out measurements from 5×10^{-2} to 3×10^{6} Hz. The measurements were performed in inert N_2 atmosphere from 150 °C to −150 °C. The temperature was controlled by a nitrogen jet (QUATRO from Novocontrol) with a temperature error of 0.1 °C during every single sweep in frequency. Molded disc shaped samples of about 0.1 μm thickness and 20 mm diameter were used. Glass fiber spacers were used to ensure the stability of the samples thickness at high temperatures. In order to avoid the increase of conductivity due to the water, the samples were previously dried at 70 °C in a vacuum oven until constant weight. The experimental uncertainty was better than 5% in all cases.

3. RESULTS AND DISCUSSION

Sample Hydrophilicity Characterization. The hydrophilic character of the materials can be related to the water uptake at given conditions. The WSP parameter was evaluated by means of dipping the samples in pure water at 20 °C until constant weight. The WSPs of the samples, see Table 2, are intimately related to the molar ratio of hydrophilic to hydrophobic monomers comprising the sample. Figure 1 shows the influence of the VP content, which contains the highly hydrophilic lactam structure, on the WSP. The water swelling of the sample with 100% of VP, i.e., 100VP/0BA, is so high that the sample loses all its mechanical properties in the swollen state. Thus, the measurement of the WSP cannot be carried out accurately because the measure is subject to large errors and, consequently, a single exact data cannot be provided. Nevertheless, for indicative purposes, we have shown in Figure 1 three different WSP values obtained with the same 100VP/0BA sample.

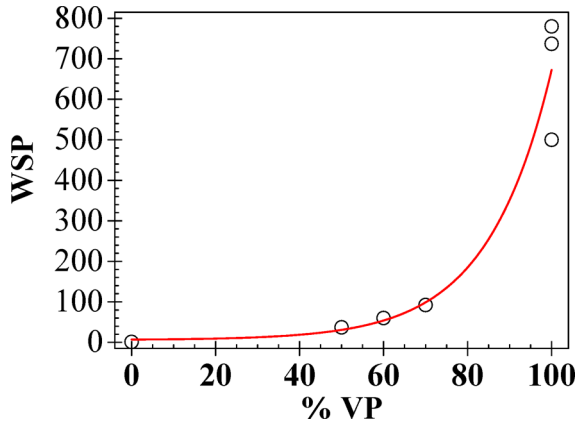

Figure 1. Influence of the mole percentage of the hydrophilic VP monomer on the hydrophilic character of the samples.

The influence of water in the physical properties of materials having 2-pyrrolidone moieties will be discussed in the next sections. Moreover, Tan et al. developed a study of the T_g depression of PVP in relation to the water uptake.[4]

Fourier Transform Infrared Measurements (FTIR). The FTIR spectra of the *x*VP/*y*BA samples showed the characteristic absorption bands corresponding to the functional groups present in the chemical structure of the material. The assignment of these bands is depicted in Figure 2, parts a and b. The band at 3400 cm^{-1} corresponds with the OH stretching of the water molecules absorbed by the samples from the environment. As expected, the intensity of this band increases with the VP content. The two $\nu_{C=O}$ bands were ascribed to (i) the majority pendant lactam structure (lower energy band, amide I), and (ii) the pendant butyl ester structure together with the cross-linker agent (higher energy band). According to the FTIR results, the chemical composition influences not only the intensity and energy of these two absorption bands, but also the transmittance ratio between the bands. While the higher energy band absorption maxima (1727 cm^{-1}) was not affected by the copolymer composition, the absorption maxima of the amide I band shifted to higher energies with BA content. Thus, the amide I ($\nu_{C=O}$) absorption maxima of the 100VP/0BA sample, observed at 1650 cm^{-1}, was shifted to 1678 cm^{-1} for the 50VP/50BA sample. This shift showed a nearly linear correlation with the chemical constitution of the samples, as shown in Figure 2c. These facts can be ascribed to the different nature of the ester and amide (lactam) groups. While the former does not establish strong interactions between them, the later establishes relatively strong permanent dipole−dipole interactions (see Figure 3). Hence, within the 100VP/0BA sample structure there are strong and highly directional dipole−dipole bond interactions in-between the pendant lactam subgroups.[6] Upon random copolymerization, these permanent dipole−dipole interactions are impaired because these groups are moved away from each other giving rise to an increase in the C═O bond strength.

In order to deepen into the nature of water/sample interaction of our systems, a FTIR analysis of dry and swollen samples was carried out. Thus, Figure 4a shows the normalized FTIR spectra of dry and swollen 50VP/50BA sample as an example. The experimental spectrum of water and the theoretical composite spectrum of water swollen 50VP/50BA system, i.e., the mathematical addition of the water and the dried 50VP/50BA sample spectra, are also represented. As it is

dx.doi.org/10.1021/ma500800a | Macromolecules 2014, 47, 5334−5346

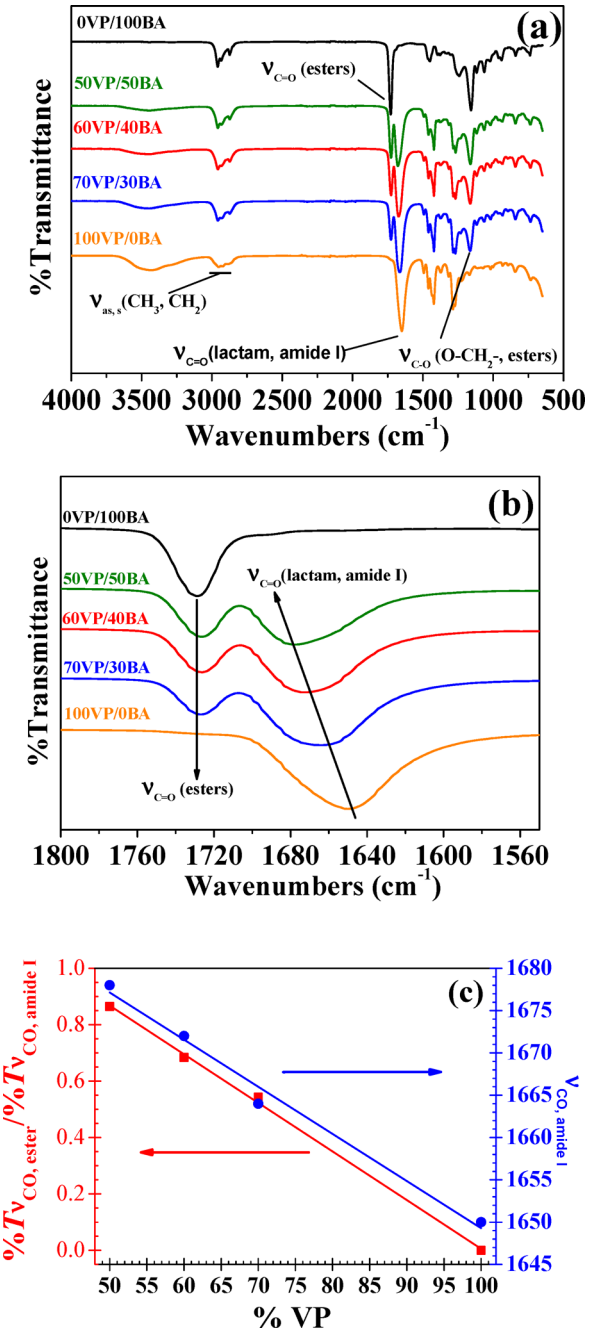

Figure 2. (a and b) Normalized FTIR spectra of the samples. (c) Correlation between the percentage of VP and (i) transmittance ratio of the peaks corresponding to the C═O of the pendant ester and lactam residues and (ii) maximum wavenumber of the stretching band corresponding to the C═O of the lactam residue.

observed, the $\nu_{C=O}$ (ester) band corresponding to the BA moieties does not shift upon swelling the samples, meaning a negligible interaction with water. On the other hand, the $\nu_{C=O}$ (lactam, amide I) band shifted to lower energy wavenumbers, pointing out a weakening of the C═O bond because of the hydrogen bonds formation with water (Figure 3**c**). The shift of this band to lower wavenumbers in the swollen samples, δ, is consistent with the hydrophilic character of the samples (δ = 24, 30, and 32 cm^{-1} for 50VP/50BA, 60VP/40BA, and 70VP/30BA, respectively). This fact is clearly observed in Figure 4**b** where the composition 50VP/50BA is represented.

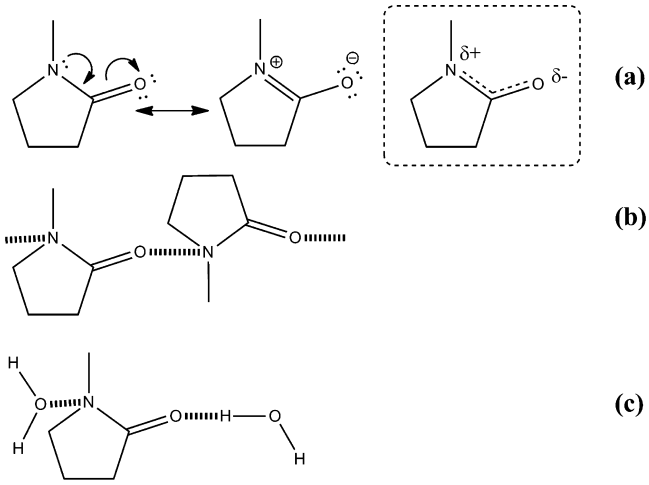

Figure 3. (a) Structure of 2-pyrrolidone moieties. (b) Model of dipolar 2-pyrrolidone/2-pyrrolidone interactions. (c) Model of 2-pyrrolidone/water interactions.

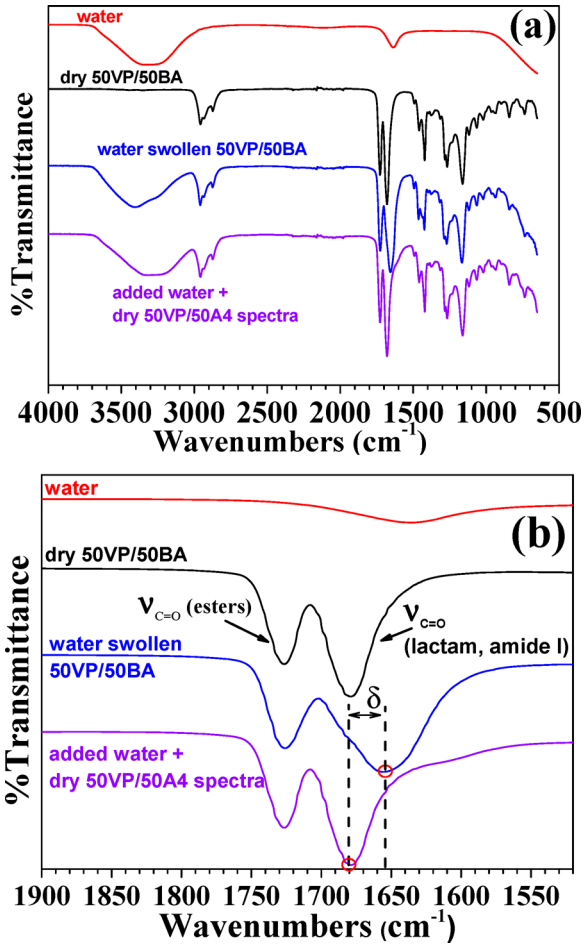

Figure 4. Normalized FTIR spectra of (a) pure water, 50VP/50BA sample (dry and water swollen), and theoretical composite spectrum of water swollen 50VP/50BA sample (mathematical addition of the water and the dried 50VP/50BA spectra) and (b) zoom of the $\nu_{C=O}$ of ester and lactam, amide I bands.

Thermogravimetric Analysis (TGA). The thermal stability of the *x*VP/*y*BA samples was evaluated using TGA. Figure 5a shows the TGA spectra obtained for the *x*VP/*y*BA samples. Table 2 shows the thermal resistance under dynamic

dx.doi.org/10.1021/ma500800a | *Macromolecules* 2014, 47, 5334−5346

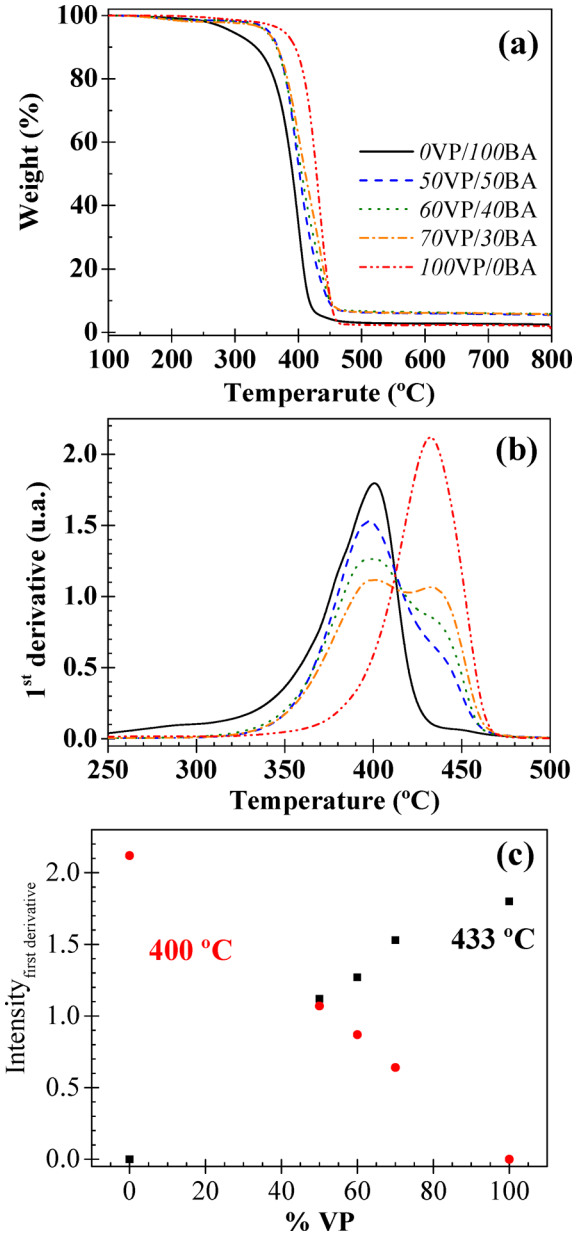

Figure 5. (a) TGA curves of the *x*VP/*y*BA samples (weight loss as a function of the temperature under inert atmosphere, N_2). (b) First derivative of the TGA curves ($\Delta_{\text{weight loss}}/\Delta_{\text{time}}$) and (c) the % VP vs the maxima intensity of the first derivative at 400 °C (circle) and 433 °C (square).

conditions, in terms of the temperature at which a weight loss of 5% and 10% is observed (T_5 and T_{10} respectively). The results clearly show the great influence of the copolymer structure. Thus, the best thermal performance is observed for 100VP/0BA homopolymer, while the worst behavior was obtained for 0VP/100BA homopolymer. This is probably because (i) the amide bonds are stronger than the ester ones, (ii) the lactam structure is prone to establish relatively strong and highly directional inter and intrachain dipole−dipole interactions, and (iii) thermal breakage of a single bond of the lactam, which is a cycle, does not give rise to the loss of a detectable low-mass fragment.

Figure 5b shows the first derivative of the degradation curves ($\Delta_{\text{weight loss}}/\Delta_{\text{time}}$), where the different thermal resistance of the samples can be analyzed. This figure exhibits one peak for the homopolymers and two peaks for the copolymer samples. Each pendant residue gives rise to a well-defined maximum degradation rate. For the copolymer samples, the highest weight loss rate observed at about 400 °C corresponds to the degradation of the ester residue and the second one observed about 433 °C is attributed to the lactam subgroup degradation. Figure 5c shows the relative weight loss rate of each subgroup (intensity first derivate) which is proportional to the molar rate of these structural units.

Differential Scanning Calorimetry Measurements. The DSC thermograms (reversing curves) obtained for all the samples are plotted in Figure 6. The characteristic T_gs and their associated heat capacity changes are summarized in Table 3.

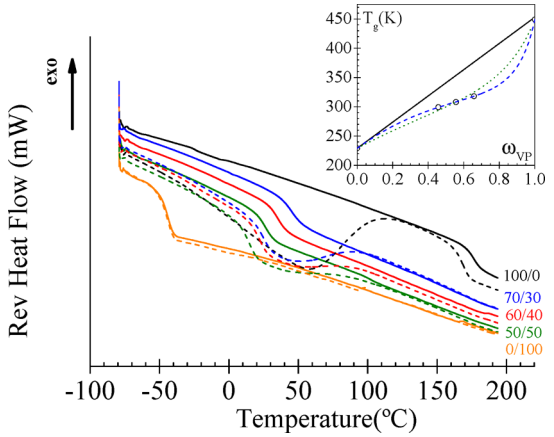

Figure 6. DSC experimental curves for *x*VP/*y*BA samples: (i) 1st heating ramp (dashed lines) and (ii) 2nd heating ramp (continuous lines). Data are vertically shifted for a better visualization. Inset: Experimental T_g as a function of VP content (circle) and T_g values predicted by the behavior based on the simple weight function (—), by the Gordon−Taylor (– –) and by the Kwei (···) equations.

It is well-known that hydrophilic polymers can absorb water (moisture) from the atmosphere. Thus, DSC was also used to monitor the drying process. Evaporation of the moisture gives rise to a broad endothermic peak in the nonreversing curve. This peak is quite broad because water evaporation takes place over a wide range of temperatures. The presence of water in polymers is known to act as a plasticizer, decreasing the T_g. For *x*VP/*y*BA samples with x = 100, 70, 60 and 50, the first heating ramp exhibits this endothermic peak at about 100 °C. From the evaporation heat of bulk water (2400 *J*/*g* at 100 °C), the amount of moisture present in samples was estimated. The moisture percentages are collected in Table 3. As it is observed, the humidity increases with the VP content, due to the formation of hydrogen bonds between water molecules and 2-pyrrolidone units (Figure 3c).

All DSC thermograms present a first step related to the glass rubber transition temperature. Prior to polymerization, the two monomers were visually miscible. Thus, the presence of one T_g in the copolymers is indicative of this miscibility (Figure 6). The observed step for each sample occurs at lower temperatures in the first heating ramp, due to the plasticizing effect of water. For all the analyzed copolymers, the obtained T_gs range between the homopolymers T_g values. These results obtained for the homopolymers match with the data acquired by conventional DSC, which were published in previous works.[18−23] The T_g values for the copolymer samples decrease monotonously with the BA content, as expected due to the

dx.doi.org/10.1021/ma500800a | *Macromolecules* 2014, 47, 5334−5346

Table 3. Characteristic Temperatures, Heat Capacity Change, and Moisture of *x*VP/*y*BA Samples

	0VP/100BA	50VP/50BA	60VP/40BA	70VP/30BA	100VP/0BA
T_g^{DSC}, °C (K)[a]	−44.11 (229)	26.24 (299)	35.02 (308)	45.13 (318)	176.18 (449)
T_{on}, °C[a]	−49.22	20.49	28.76	36.97	170.72
T_{end}, °C[a]	−40.13	31.47	41.87	53.21	180.83
ΔT, °C[a]	9.09	10.98	13.11	16.24	10.11
ΔC_p, J/g °C[a]	0.2751	0.1634	0.1627	0.1588	0.1572
T_g^{DRS},°C (K)[c]	−50 (223)	27 (300)	34 (307)	50 (323)	—
moisture,[b] %	0.0	3.0	3.8	6.3	12.2

[a]Values of characteristic temperatures and heat capacity change corresponding to the 2nd heating ramp. [b]Percentage of moisture corresponding to the 1st heating ramp. [c]At which τ_{max} (α^{DRS}) = 1 s. For 0VP/100BA homopolymer, the value was taken from ref 39.

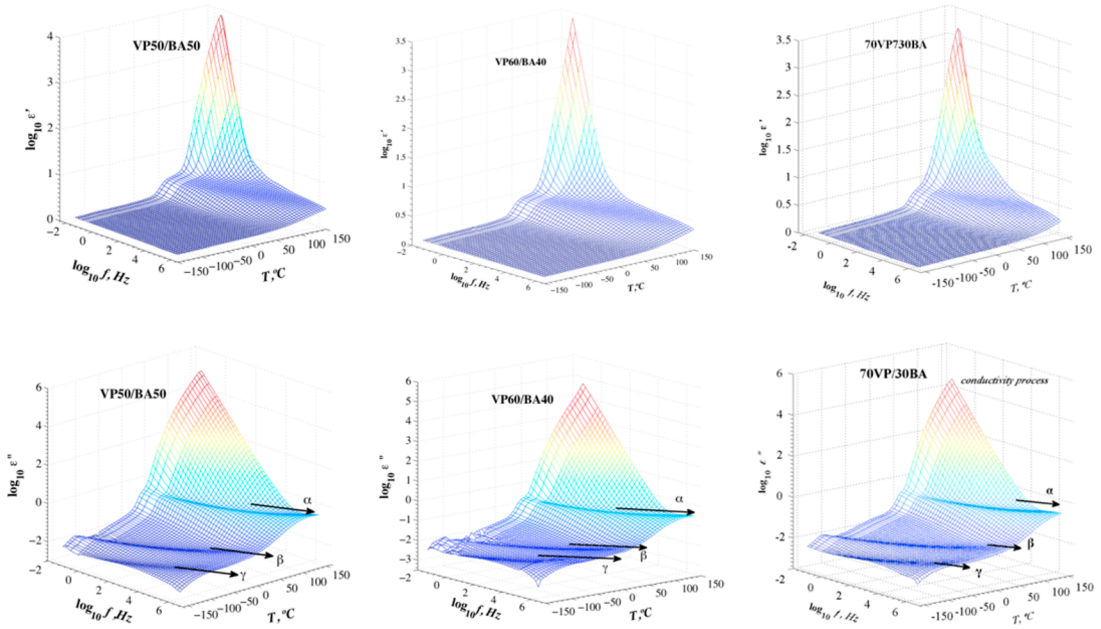

Figure 7. 3D representation of the dielectric permittivity of *x*VP-*y*BA copolymer samples in the temperature range of +150 °C to −150 °C at 5 °C steps.

plasticizing effect of the butyl units on the *x*VP/*y*BA mobility. Moreover, according to the FTIR results, the specific permanent dipole−dipole interactions between VP chains probably reduce the available free volume, decreasing the mobility in the *x*VP/*y*BA samples. The inset of Figure 6 shows the experimental dependence of T_g with the VP content, as well as the values predicted by different models. The most basic model is the so-called simple weight function, defined as $T_g = \omega_{VP}T_{gVP} + \omega_{BA}T_{gBA}$, where T_g,T_{gVP}, and T_{gBA} are, respectively, the T_gs of the copolymer sample, VP homopolymer, and BA homopolymer and ω_{VP}, ω_{BA} are the corresponding weight fractions. As is observed in Figure 6, the experimental behavior was not adequately predicted by this model. The dependence of the T_g with composition in *x*VP/*y*BA samples shows a negative deviation respect to this simple weight function.

When there are deviations from the simple weight function, several classical equations can correlate and/or predict the dependence between the T_g of a miscible system and its composition. One of them is the Gordon−Taylor equation, $T_g = (\omega_{VP}T_{gVP} + k\omega_{BA}T_{gBA})/(\omega_{VP} + k\omega_{BA})$,[24] where k is the ratio between the volume expansion coefficients of the homopolymers. Another one is the Kwei empirical equation $T_g = ((\omega_{VP}T_{gVP} + k\omega_{BA}T_{gBA})/(\omega_{VP} + k\omega_{BA})) + (q\omega_{VP}\omega_{BA})$,[25] where the quadratic term, $q\omega_{VP}\omega_{BA}$, is assumed to be proportional to the number of specific interactions between the polymer chains.[25,27] So, the q value from the Kwei equation can be used to estimate the strength of the interchain interactions. The values k =7.2 ± 0.1 and q =189.6 ± 2.4 K of the Kwei equation were determined by the least-squares procedure to obtain the best fit to the experimental points. Only the model of Kwei could fit the experimental data, since it takes into account the interchain interactions occurring in the samples and supported by the FTIR results. Therefore, the negative deviation of the simple weight function is indicative of interchain interactions, which decrease the mobility of the polymer chains. Negative deviation was already previously encountered in copolymer samples presenting very strong dipole−dipole and hydrogen-bonding interactions.[25,28−33]

The width of the glass transition may reflect the magnitude of local compositional fluctuations in the copolymer samples, giving a qualitative implication of the relative homogeneity of the system.[34] In our case, the broadening of the glass transition ($\Delta T_g = T_{end} - T_{on}$) is lower for the extreme compositions (homopolymer samples). However, for the intermediate compositions, ΔT_g is only slightly higher and increases with the VP content. This broadening of the glass transition is due to small-scale compositional fluctuations in the copolymer.

On the other hand, the heat capacity jump at T_g, ΔC_p, for the *x*VP/*y*BA copolymer samples ranges between the ΔC_p values of the homopolymers. Moreover, these values for the *x*VP/*y*BA

dx.doi.org/10.1021/ma500800a | Macromolecules 2014, 47, 5334−5346

copolymer are similar to that obtained for the 100VP/0BA sample. As the comportment of T_g, the ΔC_p versus composition showed negative deviation from the linear behavior. This tendency has been observed in systems which exhibit segmental interactions.[26,29] Thus, the composition dependence of the ΔC_p can be related to the presence of orderly packing of polymer molecules, which lowers the mobility at T_g. The ΔC_p value might include enthalpy contribution from the breaking of dipole−dipole bonds during heating.

Mechanical Properties. There is always a relationship between the mechanical properties and the chemical constitution of every material. In our case, the 100VP/0BA sample was hard and brittle. However, the 0VP/100BA sample was soft, and had to be prepared with a thickness three times higher than the others in order to obtain a manageable material. The copolymer samples showed a mechanical behavior in-between the properties presented by 100VP/0BA and 0VP/100BA homopolymers. Moreover, from a macroscopically point of view, they were highly tractable materials. The properties of the samples are shown in Table 2. The Young modulus and the tensile strength increase with the VP content, whereas the elongation (%) decreases with the VP content. These tendencies are related to the increase of the hardness and brittleness of the samples with the VP content.

Dielectric Measurements. Conductivity process can be increased by the moisture of the sample, so the dipolar processes may be hidden. Therefore, all the samples were previously dried to eliminate the absorbed moisture from the air.

Figure 7 shows the temperature and frequency dependence of the dielectric permittivity and loss factor for the *x*VP/*y*BA copolymer samples. For all samples, the dielectric permittivity ε' displays the same pattern for all isochrones. It is observed a low temperature step associated with the glass rubber transition, or α relaxation process, followed by an important increase of the permittivity. This increase is related to the electrode polarization (EP), coming from the accumulation of charges at the electrode-polymer interface.

On the other hand, the dielectric loss factor spectra clearly present two relaxational zones. In the low-temperature zone, we can observe two secondary relaxations, labeled as γ and β processes, presumably associated with local side chain motions. In the high-temperature zone, the spectra present an ostensible α relaxation and a process associated with the EP conductivity phenomenon.

The analysis of the dielectric spectra, in the frequency domain, was made by using the empirical equation of Havriliak−Negami (HN)[35−37] which relates the complex permittivity (ε^*) to the frequency by

$$\varepsilon^*_{dip}(\omega) = \varepsilon_\infty + \frac{\varepsilon_0 - \varepsilon_\infty}{[1 + (j\omega\tau)^a]^b} \quad (1)$$

where $\omega = 2\pi f$ is the angular frequency, the subscripts ε_0 and ε_∞ are, respectively, the relaxed ($\omega = 0$) and unrelaxed ($\omega = \infty$) dielectric permittivities, and τ is the relaxation time of the process. The shape parameters a and b fulfill the condition $0 < ab \leq 1$, and for a Debye process $a = b = 1$. The parameter a is related to the departure of the complex ε'' *vs* ε' plot from a semicircumference at low frequencies, the lower the a-parameter, the higher the departure is. In the ε'' spectrum, this parameter is related to the peak width, the higher the a-parameter, the narrower the peak is. The parameter b is related to the skewness of the plot along a straight line, at high frequencies. For secondary absorptions, the b parameter is equal to one. The fit was carried out in two different zones in order to facilitate the characterization of the dipolar and conductive processes. As an example, the deconvolution procedure is depicted in Figure 8 for high (conductivity and α processes) and low (β and γ processes) temperature zones.

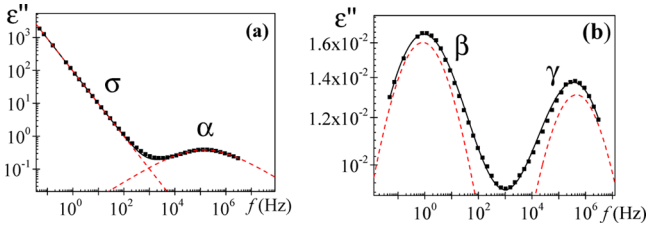

Figure 8. Deconvolution of loss factor for 50VP/50BA (a) conductivity and α processes at 90 °C and (b) β and γ processes at −110 °C. Squares represent the experimental data, continuous line the HN fitting curve, and dashed lines the individual processes.

In the low temperature zone, an additive rule for the permittivity was assumed for the analysis of the dielectric loss spectra of the secondary processes.[38]

$$\varepsilon''_{dip}(\omega) = \mathrm{Imag}\left[\sum_{i=1}^{2} \frac{\Delta\varepsilon_i}{[1 + (j\omega\tau_i)^{a_i}]^{b_i}}\right] \quad (2)$$

The HN parameters of the two secondary relaxations were determined at several temperatures from a multiple nonlinear regression analysis of the experimental data. The three characterizing peak parameters ($\Delta\varepsilon_i$, τ_i, a_i) were allowed to vary and are plotted in Figures 9 −11.

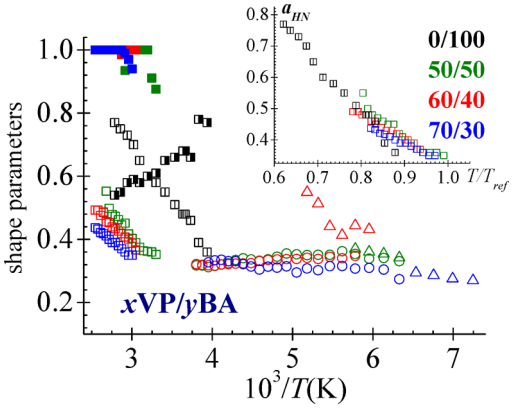

Figure 9. Temperature dependence of the shape parameters a_{HN} (open symbol) and b_{HN} (full symbol) for α (squares), β (circles), and γ (triangles) relaxations. For the secondary processes, $b_{HN} = 1$. For the 0VP/100BA: a_{HN} (square with vertical bar) and b_{HN} (▮). Inset: a_{HN} parameter for α-process as a function of normalized temperature [T_{ref} is the temperature which the $\tau_{max}(\alpha) = 1$ s].

In the high temperature zone, where the conductive process is dominant, we have included a new term in order to characterize the spectra: $\varepsilon^*(\omega) = \varepsilon^*_{dip} + \varepsilon^*_{cond}$ with $\varepsilon^*_{cond}(\omega) = j(\sigma/e_0\omega^s)$ where e_0 is the permittivity of free space (e_0= 8.854 pF·m^{-1}), σ is the conductivity arising from charges transport at the liquid-electrode interface and s is a constant ($s \leq 1$). The fit parameters determined at several temperatures from a multiple nonlinear regression analysis are summarized in Figures 9−11.

dx.doi.org/10.1021/ma500800a | *Macromolecules* 2014, 47, 5334−5346

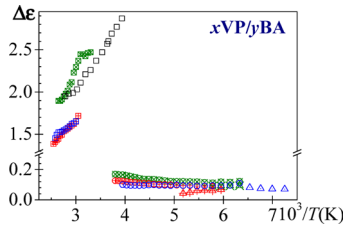

Figure 10. Temperature dependence of the strengths of the α (squares) (0/100 (□), 50/50 (square with ×), 60/40 (⊞), 70/30 (⊡)), β (circles) (50/50 (⊗), 60/40 (⊕), 70/30 (⊙)) and γ (triangles) (50/50 (triangle with an ×), 60/40 (triangle with a plus), 70/30 (triangle with a center dot)) relaxations of xVP/yBA samples.

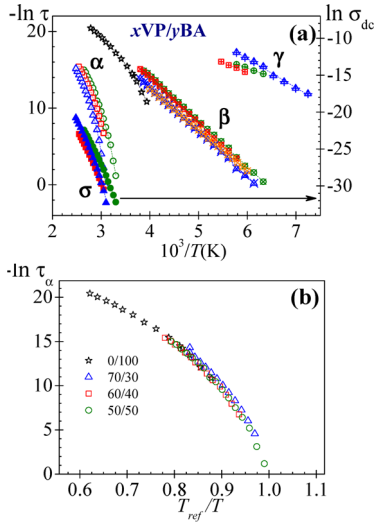

Figure 11. (a) Temperature dependence of the relaxation times for xVP/yBA samples in the left Y-axis: α (0/100 (☆), 50/50 (○), 60/40 (□), 70/30 (Δ)), β (50/50 (⊗), 60/40 (square with an ×), 70/30 (triangle with an ×), 100/0 (pentagon with an ×)) and γ (50/50 (⊕), 60/40 (⊞), 70/30 (triangle with a plus)) dipolar relaxations. Temperature dependence of the ionic conductivity for xVP/yBA samples in the right Y-axis [50/50 (●), 60/40 (■), 70/30 (▲)]. Lines represent the fitting. (b) Relaxation time for α-process as a function of normalized temperature.

Figure 9 shows the temperature dependence of the shape parameters associated with all relaxation processes present in the xVP/yBA samples. The a_{HN} parameter is a function of temperature and composition. For the α relaxation, the value of a_{HN} parameter increases with temperature, which is an indication of the decrease of the homogeneity. The shape parameters of the 0VP/100BA homopolymer were taken of the Fioretto paper.[39] The a_{HN} parameter values increase with the VP content, but they are similar after normalization by $T_{ref} = T_g$ (inset Figure 9). This is an indication of both, the homogeneity and the insignificance of the concentration fluctuation effect in the xVP/yBA series. Moreover, the value of b_{HN} parameter was near to one at all temperatures investigated for the copolymer samples. Thus, eq 1 reduces to the Cole−Cole equation[40] that describes a relaxation with a symmetric distribution of relaxation times. For amorphous polymers, a nonsymmetric distribution of times is expected for the α relaxation, associated with macromolecular segmental motion at temperatures immediately above the T_g. But for semicrystalline polymers and more generally for heterogeneous systems, a symmetrical distributions were observed for the α relaxation processes.[41−49]

However, the a_{HN} parameter for the β process is very similar for all xVP/yBA copolymers samples, and slightly decreases with the increase of temperature. For the γ process, the a_{HN} parameter increases by increasing temperature. Finally, for both secondary processes, the b_{HN} parameter was fixed to one in the fitting procedure,.

The temperature dependence of the relaxation strength is shown in Figure 10. For β and γ processes, this dependence follows the classical trends, that is, the dielectric strength increase or nearly remain constant with the temperature. This fact is consistent with a thermally activated mechanism because the dipole mobility rises with the temperature, associated with the free volume increase. Nonsignificant changes in the dielectric strength for the β and γ absorptions with the composition are observed. Nevertheless, the α-relaxation strength decreases with temperature. The thermal energy disturbs the alignment of the molecule dipoles that intervene in the cooperative motions and give rise to the relaxation. One should expect that the dielectric strength increases with VP content, reflecting the increasing polarity of the polymer chains. However, the experimental trend of the dielectric strength is at odds with this last assumption. This behavior can be related to the reduction in the molecular mobility as the VP content increases. As mentioned before (FTIR results), the mobility impairment can be caused by the presence of dipole−dipole interactions between the lactam groups present in the structural unit of VP.

The temperature dependence of the relaxation times, which is associated with the peak maxima of the primary and secondary absorptions, is shown in Figure 11a. According to our results, the increase of VP content results in an increase of the T_g and segmental relaxation times of the xVP/yBA samples. As usual, the average relaxation time associated with the α-relaxation is described by the Vogel−Fucher−Tamman−Hesse (VFTH) equation.[50−54] The deviation of the α relaxation from the Arrhenius behavior may be quantified by the strength coefficient D_0 in a modified form of the VFTH equation given by

$$\tau = \tau_0 \exp\left(\frac{D_0 T_v}{T - T_v}\right) \quad (3)$$

where τ_0 is a prefactor of the order of picoseconds and T_v is the Vogel temperature currently associated with the temperature at which the entropies of the glassy systems and the crystal are similar; i.e., the configurational entropy of the glass system is nil. Values of the τ_0, T_v, and D_0 parameters that fit eq 3 to the experimental results are collected in Table 4 for all xVP/yBA copolymer samples. As usual, the values of T_v are nearly 50 °C below those of T_g. Moreover, the strength coefficient obtained for these samples are lower than 10, the frontier that separates fragile ($D_0 < 10$) from strong ($D_0 > 10$) glasses.[55−57]

By comparing eq 3 with the Doolittle expression,[58,59] the relative free volume $\phi_g/B = (T_g - T_v)/(D_0 T_v)$ and the expansion coefficient of the free volume $\alpha_f = 1/(D_0 T_v)$ at T_g were evaluated (see Table 4). Free volume theories require that the ratio of the activation energy at constant volume to that at constant pressure is zero. However, this ratio for polymers is not zero,[60] which questions the applicability of these theories to the α-relaxations. Even so, it is an experimental fact that the values of the ϕ_g/B and α_f for most flexible polymers lie in the vicinities of $2.5 \times 10^{-2} \pm 5.0 \times 10^{-3}$ and $(4-6) \times 10^{-4}$ K^{-1}, respectively.

dx.doi.org/10.1021/ma500800a | Macromolecules 2014, 47, 5334−5346

Table 4. Characteristic Parameters of the Dipolar and Conductivity Processes of the *x*VP/*y*BA Samples

	0VP/100BA	50VP/50BA	60VP/40BA	70VP/30BA	100VP/0BA
			γ-Process		
$\log_{10}\tau_\infty$, s	-11.5 ± 0.4^a	-12.6 ± 0.3	-13.3 ± 0.3	-14.1 ± 0.5	—
E_a, kJ·mol^{-1}	12.1 ± 0.3^a	19.2 ± 0.8	22.1 ± 1.0	25.2 ± 1.3	—
$(E_{a\gamma}/RT_g)_{expt}$	4.4	7.7	8.6	9.5	—
$(E_{a\gamma}/RT_g)_{cal}$	6.9	9.2	11.2	13.0	—
			β-Process		
$\log_{10}\tau_\infty$, s	—	-16.5 ± 0.1	-16.4 ± 0.1	-15.6 ± 0.1	-14.7 ± 0.1^b
E_a, kJ·mol^{-1}	—	49.4 ± 0.2	49.5 ± 0.2	47.7 ± 0.4	44.4 ± 0.9
$(E_{a\beta}/RT_g)_{expt}$	—	19.1	19.1	16.4	—
$(E_{a\beta}/RT_g)_{cal}$	—	18.6	18.4	17.8	—
			α-Process		
$\log_{10}\tau_0$, s	-12.0 ± 0.5^c	-10.9 ± 0.2	-11.2 ± 0.1	-10.5 ± 0.1	—
D_0	7.2 ± 1.3^c	5.5 ± 0.4	5.9 ± 0.2	4.2 ± 0.1	—
T_v, K	178 ± 7^c	246.5 ± 2.8	249.5 ± 1.8	275.3 ± 1.1	—
ϕ_g/B	0.040 ± 0.004	0.039 ± 0.003	0.040 ± 0.003	0.037 ± 0.002	—
$\alpha_f \times 10^4$, K^{-1}	7.8 ± 1.1	6.6 ± 0.4	6.4 ± 0.6	5.8 ± 0.4	—
m	49.2 ± 5.0	58.4 ± 4.0	56.8 ± 4.5	60.0 ± 4.0	—
m*	73.1	93.0	95.5	99.5	134.8
$E_a(T_g)$, kJ·mol^{-1}	216 ± 23	335 ± 28	335 ± 26	365 ± 24	—
E_a*(T_g), kJ·mol^{-1}	279	502	534	572	1176
β_{KWW} [at T_g]	0.15	0.23	0.24	0.27	—
			Ionic Conductivity Process		
$\log_{10}\sigma_0$, S·cm^{-1}	—	-2.8 ± 0.4	-2.8 ± 0.2	-2.2 ± 0.3	—
D_0	—	16.8 ± 1.8	18.5 ± 0.4	14.7 ± 1.6	—
T_0, K	—	182.9 ± 5.6	185.2 ± 1.2	208.0 ± 5.9	—

[a]Reference 61. [b]Reference 62. [c]Reference 39.

In Table 4, the VTFH parameters corresponding to 0VP/100BA homopolymer were taken from the literature.[39,61] We do not have any evidence of available data regarding α-relaxation process for dry PVP in the literature. In Table 4, the parameters associated with the β process are those one corresponding to the PVP with low water content (1 wt %) reported by Cerveny and co-workers.[62]

According to our results, for all *x*VP/*y*BA copolymer samples the obtained ϕ_g/B parameter is slightly higher than the indicated average value found in most flexible polymers.[63] On the other hand, the results for α_f value are in agreement with those reported for other flexible polymers.[63]

Angell[64] introduced in the 1980s the concept of dynamic fragility. This parameter rationalizes the deviation of supercooled liquids from Arrhenius behavior in the vicinity of the T_g, for the α-relaxation. The dynamic fragility index, m, is an index of the cooperative motions in polymers that are influenced by intermolecular interactions. It characterizes how rapidly the properties vary when the temperature of a supercooled liquid approaches its T_g and it is defined as[65−67]

$$m = \lim_{T \to T_g} \left[\frac{\mathrm{d}[\log \xi]}{\mathrm{d}(T_g/T)} \right] \tag{4}$$

where ξ may be the viscosity η or the relaxation time τ of the α absorption. Fragile polymers have a high slope because ξ intensely changes through the reference temperature, consequently a dramatic departure from the Arrhenius behavior is observed. On the other hand, strong polymers show a slight deviation from the Arrhenius behavior, maintaining their properties in the transition region. Taking τ_g as reference and considering the temperature dependence of the α relaxation for flexible polymers and liquids governed by eq 3, the fragility parameter can be written as

$$m = \frac{D_0 T_v}{2.303 T_g (1 - T_v/T_g)^2} \tag{5}$$

Fragility values typically range between m = 16, for strong systems, and m = 200 for the fragile ones.[68] The values of m, collected in Table 4, show that, for the *x*VP/*y*BA copolymer samples the dynamic fragility index slightly increases with the respective T_g. This trend is in agreement with Angell's energy landscape model.[55,69] If the density of minimum energy is high in the hypersurface, the material will have a larger probability of finding a new conformation and thus will exhibit higher fragility. Fragile materials usually have a higher degree of intermolecular coupling (i.e., high cooperativity) which is quickly lost with rising temperature, so that the relaxation process changes rapidly. The rapid change of conformation suggests a larger entropy change, or large ΔC_p. However, correlation between dynamic fragility index and ΔC_p is not present in all polymeric systems.[70,71]

In *x*VP/*y*BA copolymer samples, it is observed that larger ΔC_p (T_g) is associated with more fragile behavior, also in agreement with Angell's energy landscape model.[55,69] However, the VP and BA homopolymers show a different behavior from this model. On the one hand, the BA homopolymer shows the lower fragility but it has the higher ΔC_p. This behavior has been observed in some systems where the formation of nanodomains, integrated by the side chains flanked by the backbone, is produced.[10,11] This effect can be understood in terms of decreasing free volume. Thereby, larger ΔC_p values does not necessary imply higher fragility. ΔC_p might include enthalpy contribution associated with rearrangement of the molecular chains, which leads to the formation of side chain nanodomains.

dx.doi.org/10.1021/ma500800a | Macromolecules 2014, 47, 5334−5346

On the other hand, due to the fact that fragility is proportional to the T_g, VP homopolymer shows the highest fragility. Nevertheless, this sample has the lowest value of ΔC_p,[72] tendency observed in some hydrogen-bonded systems.[73] We do not have information on this parameter for the 100VP/0BA sample because the conductive contribution to permittivity masks the α-relaxation process (see Figure 7). Moreover, as mentioned before, there is not available data regarding α-relaxation process for dry PVP in the literature.

Figure 11b shows the normalized temperature dependence of τ_α, also called fragility plot, for xVP/yBA samples. As it is observed, their temperature dependence is equivalent, namely, nonsignificant differences in fragility are produced between the copolymer samples. Since the fragility is related to the cooperativity, these results point out that the VP composition does not produce significant changes in cooperativity of the samples.

Qin and McKenna[72] compiled literature data for dynamic fragility of different types of glass forming liquids. They found a roughly linear increase of m with T_g for the various types of systems analyzed. The pertinent expressions were $m^* \approx 0.28(\pm 0.067)T_g + 9(\pm 20)$ for polymers and $m^* \approx 0.25(\pm 0.059)T_g + 16(\pm 10)$ for organic and inorganic ionic glasses and hydrogen bonding organics. The values of m^* calculated by the former expression for all xVP/yBA samples, are summarized in Table 4. As we can observe, although an increase tendency with T_g is reproduced, the dynamic fragility values are nearly 30% above those obtained from eq 5. The analysis of the fragility in terms of the structure, carried out by Qin and McKenna, suggests that the more flexible the polymer, the less brittle the material is and therefore, the fragility parameter (m) is lower. As it is known, the 0VP/100BA sample presents more conformational versatility that the 100VP/0BA ones, and consequently, a lower fragility parameter is expected. Exact xVP/yBA samples become more fragile with the VP content.

The apparent activation energy associated with the relaxation dynamics of the chains at T_g can be obtained from the dynamic fragility index as

$$m = \left[\frac{\mathrm{d}[\log \tau_A]}{\mathrm{d}(T_g/T)}\right]_{T=T_g} = \left[\frac{\mathrm{d}[\log \tau_{VFTH}]}{\mathrm{d}(T_g/T)}\right]_{T=T_g} \quad (6)$$

where the subscripts A and VFTH indicate, respectively, Arrhenius and Vogel relaxation times. These expressions lead to the following equation for the activation energy, $E_\alpha(T_g)$, at the T_g

$$E_\alpha(T_g) = \frac{RD_0T_V}{(1 - T_V/T_g)^2} \quad (7)$$

where R is the gas constant. By comparing eqs 5 and 7, the activation energy can be expressed by the alternative form: $E_\alpha(T_g) = 2.303RmT_g$ This relation suggests that $E_\alpha(T_g)$ is correlated with T_g in such a way that its value increases as T_g rises. Values of $E_\alpha(T_g)$ for all xVP/yBA samples are collected in Table 4. These values increase with the temperature but lie about 30% below those predicted by $E_\alpha^*(T_g) = [0.006T_g^2\ (\mathrm{K}) - 35]$ kJ/mol[74] for a wide variety of polymers.

The temperature dependence of the relaxation times associated with the secondary relaxations in the glassy state is also shown in Figure 11. According to our results, the increase in VP content results in an increase in the temperature of the maximum and in the relaxation times of the xVP/yBA samples. It can be seen that both relaxation processes follow Arrhenius behavior (ARRH) ($\tau_{max} = \tau_\infty \exp[E_a/RT]$) and their activation energies (E_a) and pre-exponential factors (τ_∞) are summarized in Table 4. It is well-known that different molecular mechanisms can be responsible for secondary processes in glass-forming materials. One type of sub-T_g relaxations involve the motion of pendant groups or an isolated part of the molecule and would be mainly controlled by intramolecular potentials. However, there is another type of sub-T_g relaxations labeled as Johari and Goldstein relaxations (JG)[75,76] that involve the motion of the whole molecule, having therefore an origin similar to that of the α-relaxation. These secondary relaxations are defined as intermolecular in character. One way to distinguish between both types of sub-T_g relaxation is to carry out the analysis proposed for Ngai, known as the coupling model (CM).[77−80] Ngai et al. found that the JG secondary relaxation obeys the following criteria: $\tau_{\beta,\gamma}(T_{g\alpha}) \approx \tau_0(T_{g\alpha}) = t_c^n\tau_\alpha^{1-n}$, where t_c is the crossover time in the CM, which is about 2 ps for small molecules and polymeric glass formers[81,82] and $n = 1 - \beta_{KWW}$ is the coupling parameter, with β_{KWW} being the stretch exponent of the KWW equation[83] that describes α relaxations

$$\phi(t) = \exp[-(t/\tau^*)^{\beta_{KWW}}] \quad (8)$$

where τ^* is a characteristic relaxation time and the stretch exponent (β_{KWW}) lies in the range 0−1 and quantifies the extent of deviation from pure exponentially, i.e., the degree of the relaxation time dispersion. The case $\beta_{KWW} = 1$ refers to simple exponential behavior.

For this purpose, the normalized α relaxation in the time domain was calculated from the retardation loss spectra[53,84] evaluated from the HN fit parameters as follows

$$\phi(t) = \frac{\int_{-\infty}^{\infty} L_\alpha(\ln \tau)\mathrm{e}^{-t/\tau}\mathrm{d}[\ln \tau]}{\int_{-\infty}^{\infty} L_\alpha(\ln \tau)\mathrm{d}[\ln \tau]} \quad (9)$$

The KWW decay functions at different temperatures are shown in Figure 12. In the inset, the respective temperature dependence of the characteristic relaxation time and the stretch exponent is shown. As usual, an increase of temperature produces a decrease in the characteristic relaxation time and an increase in the β_{KWW} value. The evolution of the τ^* with the temperature obeys the VFTH equation. The tendency of the stretch exponent can be related to the decreasing of intermolecular constraints (or coupling) between the relaxing units with increasing temperature. According to our results, the stretch exponent (β_{KWW}) decreases as the VP content increases: β_{KWW} (0VP/100BA) > β_{KWW} (50VP/50BA) > β_{KWW} (60VP/40BA) > β_{KWW} (70VP/30BA). The more VP content, the more permanent dipole−dipole interactions in the system. Thus, these permanent dipole−dipole interactions can produce intermolecular constrains between the relaxing units.

According to the CM and taking into account that (i) the T_g is conveniently defined as the temperature at which the dielectric relaxation time $\tau_\alpha \approx 1$ s and (ii) in the Arrhenius temperature dependence of the secondary relaxations, the ratio $(E_{a\beta,\gamma}/RT_g)$ can be evaluated as a function of n and τ_∞ parameters as follows[85] $(E_{a\beta,\gamma}/RT_g)_{cal} = 2.303(2 - 13.7n - \log_{10}\tau_{\infty\beta,\gamma})$. In Table 4 are collected the values of the ratio $(E_{a\beta,\gamma}/RT_g)$ evaluated by using the CM theory and from experimental data. According to our results, there is only good

dx.doi.org/10.1021/ma500800a | Macromolecules 2014, 47, 5334−5346

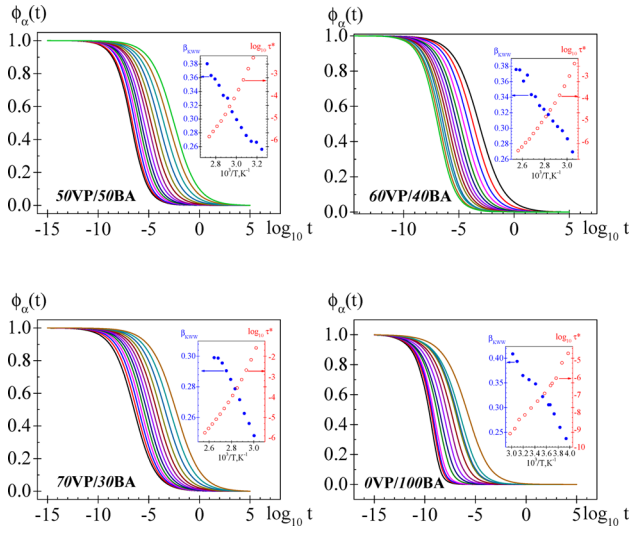

Figure 12. Normalized relaxation curves in the time domain for the α relaxation of xVP/yBA samples. The decay curves are fitted to the KWW equation using the stretch exponent β_{KWW} and the characteristic relaxation times τ^* are shown in the inset of the Figure.

agreement between the experimental value of ratio $(E_{a\beta,\gamma}/RT_g)_{expt}$ and the calculate value $(E_{a\beta,\gamma}/RT_g)_{cal}$for the slower process. This means that, the β-relaxation process is a JG process, and therefore, has intermolecular character. On the other hand, the γ-process has an intramolecular character and it is related to local motions of side chains. According to the values of the energy activation parameters (Table 4), the γ-process is related to motions of the terminal butyl units.[9,52,86] On the other hand, the β-process is related to the local motions of the pyrrolidone group accompanied by the segments motions of the polymer backbone.[9,87] The butyl unit motions responsible of the γ relaxation can be restricted by the presence of the VP units, so an increase in the activation energy of the process is observed by increasing the VP content. On the other hand, the activation energy of the β process slightly diminishes with VP content. Because of the molecular origin of β process, the motion of pyrrolidone group is restricted to the BA increasing content. However, as β relaxation is a cooperative motion, the influence of VP content in the activation energy is lower than in the γ process.

On the other hand, the ionic conductivity value obtained from the experimental data fitting procedure $(\varepsilon^*_{cond}(\omega) = j(\sigma/e_0\omega^s))$ is plotted as a function of the reciprocal of temperature in Figure 11a (right Y-axis). The temperature dependence of the ionic conductivity follows VFTH behavior $(\sigma_{dc} = \sigma_0 \exp(-D_0T_0/(T - T_0)))$, which was also found in a variety of materials.[68] The VFTH parameters deduced from the best fit are summarized in Table 4. This behavior is an indication that the origin of charge carrier transport is the segmental motions of the polymer chains.[88−90] Therefore, the conductivity process is governed by both, the free volume and the temperature.

4. CONCLUSIONS

The copolymer samples with different contents in VP and BA were chemically designed in order to improve the properties of the homopolymers. The samples were characterized by means of FTIR, TGA, DSC, mechanical, and DRS techniques. The characterization carried out shows a correlation between the properties and the chemical composition.

According to TGA and mechanical results, thermal and mechanical stability is enhanced with the VP content. The WSPs of the samples are intimately related to the molar ratio of the highly hydrophilic lactam structure (VP) to the highly hydrophobic ester residue (BA). For all samples, the DRS spectra showed three dipolar relaxations (γ, β, and α) and a conductive process specially important at low frequency and high temperatures.

The dipole−dipole interactions between amide functions,[6] which are verified by FTIR characterization, affected significantly several parameters related to the molecular mobility:

(i) The glass transition temperature. The evaluated T_gs for the xVP-yBA copolymer samples from DSC and DRS techniques are in agreement and show that the T_gs increase with the VP content due to a reduction of the molecular mobility.

(ii) The heat capacity at T_g. The higher value of the heat capacity at T_g is the corresponding to the 0VP-100BA, whereas the lower value of ΔC_p (T_g) is the obtained for the 100VP-0BA. This is related to the reduction of mobility associated with the strong dipole−dipole interactions between VP units. For the xVP-yBA copolymer samples, the ΔC_p (T_g) values are practically constant and similar to the value of 100VP-0BA sample.

(iii) The α dielectric strength values for the 50VP-50BA copolymer sample are higher than those ones obtained for the other two copolymers. This fact can be related to the dipole−dipole interactions between lactam groups that hindered the molecular motion.

(iv) The activation energy values. The activation energy of the γ process related to local butyl units motions increases with the VP content. Whereas, the activation energy of the β relaxation, which is a JG process related to the motions of the pyrrolidone group together with the polymer backbone segments, remains nearly constant with the composition. Again, these tendencies can be related to the effect of the dipole−dipole interactions in the molecular mobility.

(v) The fragility values, which are influenced by intermolecular interactions. The obtained fragility parameters indicated that these copolymers are fragile glasses. Both, the ΔC_p and the fragility index (m) increases with the VP content, already previously related to the increase in dipole−dipole interactions.[70,71]

Finally, the *dc* conductivity strongly depends on temperature and composition. The copolymer systems exhibit a VFTH behavior, which proves the contribution of segmental relaxations to conductivity.

AUTHOR INFORMATION

Corresponding Author

*(M.J.S.) Telephone: 0034963879327. E-mail: jsanchis@ter.upv.es.

Notes

The authors declare no competing financial interest.

ACKNOWLEDGMENTS

B.R.-F, M.C, P.O.-S., and M.J.S., gratefully acknowledge the CICYT for Grant MAT2012-33483. S.V., F.G. and J.M.G. acknowledge the Spanish Ministerio de Economía y Competitividad−FEDER (MAT2011-22544) and the Junta de Castilla y León (BU232U13).

REFERENCES

(1) Reppe, W. In *Polyvinylpyrrolidon*; Verlag Chemie: Weinheim, Germany, 1954.
(2) Bühler, V. *Polyvinylpyrrolidone Excipients for Pharmaceuticals: Povidone, Crospovidone and Copovidone*; Springer: Berlin, 2005.
(3) Haaf, F.; Sanner, A.; Straub, F. *Polym. J.* **1985**, *17*, 143−152.
(4) Tan, Y. Y.; Challa, G. *Polymer* **1976**, *17*, 739−740.
(5) Gallardo, A.; Lemus, A. R.; San Roman, J.; Cifuentes, A.; Diez-Masa, J. C. *Macromolecules* **1999**, *32*, 610−617.
(6) Grigoraş, V. C.; Bărboui, V. *Rev. Roum. Chim.* **2008**, *53*, 127−131.
(7) McCrum, N. G.; Read, B. E.; Williams, W. *Anelastic and Dielectric Effects in Polymeric Solids*; Dover Publications: New York, 1991.
(8) Sanchis, M. J.; Díaz-Calleja, R.; Gargallo, L.; Hormazábal, A.; Radic, D. *Macromolecules* **1999**, *32*, 3457−3463.
(9) Redondo-Foj, B.; Carsí, M.; Ortiz-Serna, P.; Sanchis, M. J.; García, F.; García, J. M. *J. Phys. D: Appl. Phys.* **2013**, *46*, 295304−295315.
(10) Carsí, M.; Sanchis, M. J.; Díaz-Calleja, R.; Riande, E.; Nugent, M. J. D. *Macromolecules* **2012**, *45*, 3571−3580.
(11) Carsí, M.; Sanchis, M. J.; Díaz-Calleja, R.; Nugent, M. J. D. *Eur. Polym. J.* **2013**, *49*, 1495−1502.
(12) Deutsch, K.; Hoff, E. A.W.; Reddish, W. *J. Polym. Sci.* **1954**, *13*, 565−582.
(13) Kalakkunnath, S.; Kalika, D. S.; Lin, H.; Raharjo, R. D.; Freeman, B. D. *Macromolecules* **2007**, *40*, 2773−2781.
(14) Kremer, F.; Schönhals, A.; In *Broadband Dielectric Spectroscopy*; Springer: Berlin, 2003.
(15) Brar, A. S.; Kumar, R. *J. Appl. Polym. Sci.* **2002**, *85*, 1328−1336.
(16) Brar, A. S.; Kumar, R. *J. Mol. Struct.* **2002**, *616*, 37−47.
(17) Miller, R. L. In *Glass transition Temperatures of Polymers, in Polymer Handbook*, 4th ed.; Brandrup, J., Immergut, E. H., Grulke, E. A., Eds.; Wiley-Interscience: Hoboken, NJ, 1999; pp VI/199.
(18) Feldstein, M. M.; Roos, A.; Chevallier, C.; Creton, C.; Dormidontova, E. E. *Polymer* **2003**, *44*, 1819−1834.
(19) Feldstein, M. M.; Shandryuk, G. A.; Kuptsov, S. A.; Platé, N. A. *Polymer* **2000**, *41* (4), 5327−5338.
(20) El-Begawy, S. E. M.; Huglin, M. B. *Eur. Polym. J.* **1991**, *27*, 1023−1027.
(21) Huglin, M. B.; Rehab, M. M. A. M. *Polymer* **1987**, *28* (13), 2200−2206.
(22) Lee, W. A., Knight, G. J. In *The Glass Transition of Polymers, Polymer Handbook*; Brandrup, J., Immergut, E. H., Eds.; Wiley-Interscience Publishers: New York, 1966; p III-66.
(23) *Properties and Behavior of Polymers*; John Wiley & Sons Ltd.: New York, March 2011; ISBN: 978-0-470-59670-8.
(24) Gordon, M.; Taylor, J. S. *J. Appl. Chem.* **1952**, *2*, 493−500.
(25) Kwei, T. K. *J. Polym. Sci.: Polym. Lett. Ed.* **1984**, *22* (6), 307−313.
(26) Anshyang, A.; Lin, T.; Kwei, K.; Reiser, A. *Macromolecules* **1989**, *22*, 4112−4119.
(27) Song, M.; Hourston, D. J.; Pollock, H. M.; Hammiche, A. *Polymer* **1999**, *40*, 4763−4767.
(28) Slark, A. T. *Polymer* **1999**, *40*, 1935−1941.
(29) Chee, K. K. *Polymer* **1995**, *36*, 809−813.
(30) Chee, K. K. *J. Appl. Polym. Sci.* **1991**, *43*, 1205−1208.
(31) Chee, K. K. *Polymer* **1987**, *28*, 977−979.
(32) Kwei, T. K.; Pearce, E. M.; Pennacchia, J. R.; Charton, M. *Macromolecules* **1987**, *20* (5), 1174−1176.
(33) Schneider, H. A. *Polymer* **1989**, *30* (5), 771−779.
(34) Bershtein, V.; Egorova, L.; Yakushev, P.; Pissis, P.; Sysel, P.; Brozova, L. *J. Polym. Sci., Part B:Polym, Phys.* **2002**, *40*, 1056−1069.
(35) Havriliak, S.; Negami, S. *Polymer* **1967**, *8* (4), 161−210.
(36) Havriliak, S.; Negami, S. *J. Polym. Sci., Part B: Polym. Symp.* **1966**, *14*, 99−117.
(37) Havriliak, S.; Negami, S. *Dielectric and Mechanical Relaxation in Materials*; Hanser: Munich, Germany, 1997; p 57.
(38) Donth, E. *J. Polym. Sci., Part B: Polym. Phys.* **1996**, *34* (17), 2881−2892.
(39) Fioretto, D.; Livi, A.; Rolla, P. A.; Socino, G.; Verdini, L. *J. Phys.: Condens. Matter* **1994**, *6*, 5295−5302.
(40) Cole, K. S.; Cole, R. H. *J. Chem. Phys.* **1941**, *9*, 341−351.
(41) Boyd, R. H. *Polymer* **1985**, *26*, 323−347.
(42) Laredo, E.; Grimau, M. *Macromolecules* **2003**, *36*, 9840−9850.
(43) Huo, P.; Cebe, P. *J. Polym. Sci., Part B: Polym. Phys.* **1992**, *30*, 239−250.
(44) Noda, N. *Polymer* **2005**, *46*, 7201−7217.
(45) Ryabov, Y.; Nuriel, H. *J. Polym. Sci., Part B: Polym. Phys.* **2003**, *41* (3), 217−223.
(46) Janik, P.; Paluch, M. *Phys. Rev. E* **2001**, *64*, 042502.
(47) Feldman, Y.; Puzenko, A.; Ryabov, Y. *Chem. Phys.* **2002**, *284*, 139−168.
(48) Ortiz-Serna, P.; Díaz-Calleja, R.; Sanchis, M. J.; Riande, E.; Nunes, R.; Martins, A.; Visconte, L. *Macromolecules* **2010**, *43*, 5094−5102.
(49) Ortiz-Serna, P.; Díaz-Calleja, R.; Sanchis, M. J.; Riande, E.; Nunes, R.; Martins, A.; Visconte, L. *J. Non-Cryst. Solids* **2011**, *357*, 598−604.
(50) Riande, E.; Díaz-Calleja, R. *Electrical Properties of Polymers*; Marcel Dekker: New York, 2004.
(51) Vogel, H. *Z. Phys.* **1921**, *22*, 645−646.
(52) Fulcher, G. S. *J. Am. Ceram. Soc.* **1925**, *8*, 339−340.
(53) Tamman, G.; Hesse, W. *Z. Anorg. Allg. Chem.* **1926**, *156*, 245−247.
(54) Lunkenheimer, P.; Schneider, U.; Brand, R.; Loidl, A. *Contemp. Phys.* **2000**, *41*, 15−36.
(55) Angell, C. A. *Science* **1995**, *267*, 1924−1935.
(56) Angell, C. A. *Complex Behavior of Glassy Systems*; Proceedings of the XIV Sitges Conference, Sitges: Barcelona, Spain, 1996.
(57) Rubi, M.; Pérez-Vicente, C. *Complex Behaviour of Glassy Systems*; Eds. Springer; Berlin, 1997.
(58) Doolittle, A. *J. Appl. Phys.* **1951**, *22* (12), 1471−1975.
(59) Doolittle, A. K. *Appl. Phys.* **1952**, *23* (2), 236−423.
(60) Mpoukouvalas, K.; Floudas, G.; Williams, G. *Macromolecules* **2009**, *42*, 4690−4700.
(61) Encinar, M.; Guzmán, E.; Prolongo, M. G.; Rubio, R. G.; Sandoval, C.; González-Nilo, F.; Gargallo, L.; Radic, D. *Polymer* **2008**, *49* (26), 5650−5658.
(62) Cerveny, S.; Alegría, A.; Colmenero, J. *J. Chem. Phys.* **2008**, *128*, 044901−044907.
(63) Ferry, J. D. *Viscoelastic Properties of polymers*, 2nd ed.; John Wiley&Sons: New York, 1961.
(64) Angell, C. A. *J. Non-Cryst. Solids* **1985**, *73*, 1−3.
(65) Bohmer, R.; Ngai, K. L.; Angell, C. A.; Plazek, D. J. *J. Chem. Phys.* **1993**, *99*, 4201−4209.
(66) Bohmer, R.; Angell, C. A. *Phys. Rev. B* **1992**, *45*, 10091−10094.
(67) Bohmer, R.; Angell, C. A. *Phys. Rev. B* **1993**, *48*, 5857−5863.
(68) Merino, E. G.; Atlas, S.; Raihane, M.; Belfkira, A.; Lahcini, M.; Hult, A.; Dionísio, M.; Correia, N. T. *Eur. Polym. J.* **2011**, *47*, 1429−1446.
(69) Angell, C. A. *J. Non-Cryst. Solids* **1991**, *131*−*133*, 13−31.
(70) Cangialosi, D.; Alegría, A.; Colmenero, J. *J. Chem. Phys.* **2006**, *124*, 024906−024909.
(71) Roland, C. M.; Santangelo, P. G.; Ngai, K. L. *J. Chem. Phys.* **1999**, *111* (12), 5593−5598.
(72) Qin, Q.; McKenna, B. *J. Non-Cryst. Solids* **2006**, *352*, 2977−2985.
(73) Santangelo, P. G.; Roland, C. M. *Phys. Rev. B* **1998**, *58* (21), 14121−14123.
(74) Rössler, E.; Hess, K. U.; Novikov, V. N. *J. Non-Cryst. Solids* **1998**, *223*, 207−222.
(75) Johari, G. P.; Goldstein, M. *J. Chem. Phys.* **1970**, *53*, 2372.
(76) Johari, G. P.; Goldstein, M. *J. Chem. Phys.* **1972**, *56*, 4411.
(77) Ngai, K. L. *J. Chem. Phys.* **1998**, *109*, 6982.
(78) Ngai, K. L.; Paluch, M. *J. Chem. Phys.* **2004**, *120*, 857−873.
(79) Ngai, K. L.; Capaccioli, S. *J. Phys.: Condens. Matter* **2007**, *19* (20), 205114.

(80) Paluch, M.; Pawlus, S.; Hensel-Bielowka, S.; Kaminska, E.; Prevosto, D.; Capaccioli, S.; Rolla, P. A.; Ngai, K. L. *J. Chem. Phys.* **2005**, *122* (23), 234506−234506−6.
(81) Ngai, K. L. *Comments Solid State Phys.* **1979**, *9*, 141−155.
(82) Ngai, K. L.; Tsang, K. Y. *Phys. Rev. E* **1999**, *60*, 4511.
(83) Williams, G. *Adv. Polym. Sci.* **1979**, *33*, 59−92.
(84) Kohlrausch, F. *Pogg Ann. Phys. Chem.* **1854**, *91*, 179−214.
(85) Ngai, K. L.; Capaccioli, S. *Phys. Rev. E* **2004**, *69*, 031501.
(86) Sanchis, M. J.; Díaz-Calleja, R.; Pelissou, O.; Gargallo, L.; Radic, D. *Polymer* **2004**, *45*, 1845−55.
(87) Zhang, S.; Painter, P. C.; Runt, J. *Macromolecules* **2004**, *37*, 2636−42.
(88) Neagu, E.; Pissis, P.; Apekis, L.; Gomez Ribelles, J. L. *J. Phys. D: Appl. Phys.* **1997**, *30* (11), 1551−60.
(89) Lu, H.; Zhang, X.; Zhang, H. *J. Appl. Phys.* **2006**, *100* (5), 054104.
(90) Smaoui, H.; Arous, M.; Guermazi, H.; Agnel, S.; Toureille, A. *J. Alloys Compd.* **2010**, *489*, 429−436.